β-delayed neutron spectroscopy of ^{70,72}Co ground-state and isomeric-state decays

K. Siegl,[1,*] A. M. Keeler,[1,†] R. Grzywacz,[1,2] N. T. Brewer,[2] B. P. Crider,[3,‡] A. Fijalkowska,[4,5] S. Go,[1] M. Hall,[6] J. H. Hamilton,[7] S. V. Ilyushkin,[8] T. King,[1] S. Liddick,[3,9] M. Madurga,[1] P. D. O'Malley,[6] S. V. Paulauskas,[1] M. M. Rajabali,[10] S. Z. Taylor,[1] E. H. Wang,[7] Z. Y. Xu,[1] and C. Zachary[7]

[1]*Department of Physics and Astronomy, University of Tennessee, Knoxville, Tennessee 37996, USA*
[2]*Physics Divison, Oak Ridge National Laboratory, Oak Ridge, Tennessee 37831, USA*
[3]*National Superconducting Cyclotron Laboratory (NSCL), Michigan State University, East Lansing, Michigan 48824, USA*
[4]*Department of Physics and Astronomy, Rutgers University, New Brunswick, New Jersey 08903, USA*
[5]*Faculty of Physics, University of Warsaw, 02-093 Warsaw, Poland*
[6]*Department of Physics, University of Notre Dame, Notre Dame, Indiana 46556, USA*
[7]*Department of Physics, Vanderbilt University, Nashville, Tennessee 37235, USA*
[8]*Department of Physics, Colorado School of Mines, Golden, Colorado 80401, USA*
[9]*Department of Chemistry, Michigan State University, East Lansing, Michigan 48824, USA*
[10]*Physics Department, Tennessee Technological University, Cookeville, Tennessee 38505, USA*

(Received 9 February 2024; accepted 7 May 2024; published 10 June 2024)

The β-decaying states of ^{70,72}Co were studied at the National Superconducting Cyclotron Laboratory using the VANDLE neutron time-of-flight array. The $(6^-, 7^-)$ β-decaying state in ^{70}Co is near-spherical with a lifetime of 113 ± 7 ms, and the low-spin $(1^+, 2^+)$ β-decaying state is postulated to be the prolate deformed ground state with a lifetime of 508 ± 7 ms. Both decay predominantly to the bound states of ^{70}Ni. For the first time neutron-emissions from neutron unbound states from both the $(6^-, 7^-)$ and $(1^+, 2^+)$ β decays were measured. Even with the low statistics data, we were able to disentangle the neutron emission from both decays, which enabled a determination of β-decay strength above the neutron separation energy of ^{70}Ni. Neutron emission probabilities were measured to be $7.1 \pm 1.5\%$ and $9.4 \pm 1.7\%$, respectively, for the $(6^-, 7^-)$ and $(1^+, 2^+)$ decays. The decay pattern of the ^{70}Co is driven by neutron $f_{5/2}$ to proton $f_{7/2}$ Gamow-Teller transformation. The observed population of neutron unbound states is attributed to the conversion of $p_{1/2}$ and $p_{3/2}$ neutrons to $p_{3/2}$ and $p_{1/2}$ protons excited across the $Z = 28$ closed shell.

DOI: 10.1103/PhysRevC.109.064309

I. INTRODUCTION

Nuclear isomers are prevalent near closed shells. One mechanism generating long-lived excited states is the proximity of orbitals with large spin differences at low excitation energy near the Fermi surface. The spherical nuclear shell model can be used to predict the properties of these nuclear isomers. As neutron number and proton-neutron asymmetry increase, nuclear structure changes occur [1]. Changes in nuclear shape may also lead to the appearance of isomeric states where spherical and deformed states coexist at low excitation.

Historically $N = 40$ has been identified as a subshell closure for nickel ($Z = 28$) isotopes [2] based on a ^{68}Ni isomer measurement. More recent measurements of ^{68}Ni and the surrounding nuclei [3–7] indicated this region as a possible site for shape coexistence. The nature of isomerism in this region becomes more complicated to interpret due to the interplay of shell and shape effects.

Measurements of the β-decay strength distribution are a standard tool to benchmark nuclear theories that aim to describe nuclear lifetimes. This is due to the sensitivity of the decay strength distribution to the nuclear structure. These studies can explain complexities that are not sufficiently captured by applying the decay selection rules. Isomers play an essential role by providing an additional test for nuclear models by exploring the role of spin or shape in β-decay strength distributions for the same nucleus [8,9]. However, not many cases have been studied because of multiple experimental challenges in providing a clean separation of ground states and isomers.

We focus here on the decay of ^{70}Co, which is produced in two β-decaying states [10–13], which have tentative spin assignments of $(6^-, 7^-)$ and $(1^+, 2^+)$ for the shorter and longer lived states, respectively. We present a new measurement of the β-decay strength distributions above the neutron separation energy in ^{70}Ni, which can explain the lifetime differences between the $(6^-, 7^-)$ and $(1^+, 2^+)$ β-decaying states in ^{70}Co.

*ksiegl@utk.edu
†Present address: Department of Radiation Oncology, Stitch School of Medicine, Cardinal Bernardin Cancer Center, Loyola University of Chicago, Chicago, IL 60660, USA.
‡Present address: Department of Physics and Astronomy, Mississippi State University, Mississippi State, MS 39762, USA.

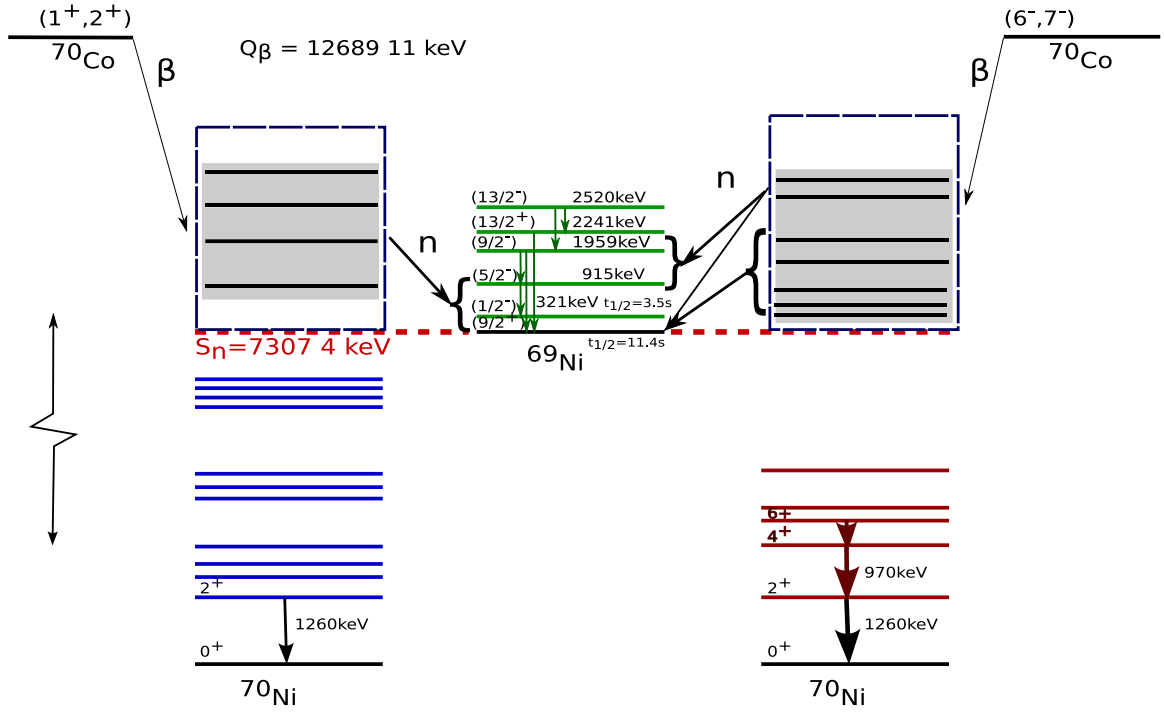

FIG. 1. The β decay of both states of ^{70}Co, the black lines above the neutron separation energy correspond to the neutron emitting unbound levels interpreted from nTOF with gray bands indicating continuum of states while the blue lines [11] and red lines [13] above ^{70}Ni correspond to some of the observed discrete levels for each decay, while the green lines above ^{69}Ni [14] are the levels calculated to be populated by neutron emission.

^{70}Co was shown to be among the impactful nuclei in an r-process sensitivity study [15] for the $N > 40$ region. Recently the role of isomers was emphasized in modeling astrophysical processes [16] with nuclear spin, excitation energy, and lifetime affecting *r*-process abundance patterns. The ^{70}Co $(1^+, 2^+)$ state was identified to be highly populated in the *r*-process network calculations, see Fig. 1 in [16].

The decay patterns of both ^{70}Co states are illustrated in Fig. 1. The decays of ^{70}Co to bound excited states in ^{70}Ni were mostly studied using high-resolution γ-ray spectroscopy. The high-spin decay has been measured numerous times. The first measurement of the low-spin decay was at Lueven using LIGLIS with the laser tuned to cobalt [10] attributing a (3^+) spherical state, and the high-spin $(6^-, 7^-)$ was also measured. Subsequent experiments at GANIL [12], and NSCL [13], further expanded the discrete levels populated by each state, and achieved new measurements of the half-lives. Most recently, the measurement at RIKEN [11] measured the low-spin decay through the decay chain of ^{70}Fe. This measurement constrained the spin and parity of the low-spin state to $(1^+, 2^+)$. The Monte Carlo shell model was applied to the low-lying states of ^{70}Co populated by the ^{70}Fe β-decay suggesting the $(1^+, 2^+)$ state was the prolate-deformed ground state of ^{70}Co, and that the $(6^-, 7^-)$ state is a near spherical isomer.

Another technique for measuring γ-ray strength in the β decay is total absorption spectroscopy (TAS) [17]. Only the decay of the $(6^-, 7^-)$ state in ^{70}Co has had a TAS measurement using the summing NaI (SuN) [18], which made a strong claim that the neutron unbound states predominantly decay via γ-ray emission. Shell-model predictions and previous detection of β-delayed neutron emission in other nuclei indicate that the β strength distribution to neutron-unbound states plays an important role. The only way to attain complete S_β information above the neutron separation energy is to also measure delayed neutron emission from the β decay. Delayed neutron emission was found for both the low- and high-spin decaying states of ^{70}Co in this experiment. The strength distribution for the decaying states differs significantly, and may be compatible with the spherical and deformed nature of the ^{70}Co states.

II. EXPERIMENT

The ^{70,72}Co implanted ions were produced by projectile fragmentation of a ^{82}Se beam at 140 MeV/nucleon on a ^{9}Be target using the A1900 fragment separator [19] at the National Superconducting Cyclotron Laboratory (NSCL). The ions were implanted in an inorganic scintillator made of the yttrium aluminum perovskite (YAP) crystal. The YAP used was 1 mm thick and 5.1 cm diameter and was affixed to a 24 × 24 segmented light-guide with 2 mm pitch, which was connected to a Hamamatsu H12700A-03 position-sensitive 64 anode photomultiplier-tube.

An Anger logic resistive network [20] was used to reduce the output channels down to a total of four for the anode signals correlated to the position of a single interaction, and a pass-through for the shared dynode signal from the position-sensitive PMT. These five signals were copied

between unamplified, and amplified signals. The implant of ions produces a large amount of light in YAP, clearly registrable in the unamplified signals. In contrast the β particle produces significantly less light and is only available in the four-times amplified signals. Location correlation of ^{70}Co implants and subsequent β decays allows the attribution of β decays to particular implants.

Delayed neutrons following β decay were observed using the Versatile Array for Detection of Neutrons at Low Energy (VANDLE) [21], which consists of 42 120-cm-long plastic scintillators. The array was positioned in a 1 m arc over the YAP detector at its center. Located below the YAP detector was a single high-purity germanium (HPGe) clover detector for high-resolution γ-ray spectroscopy, and 12 lanthanum bromide detectors for high-efficiency γ-ray detection.

The response and efficiency function of the VANDLE detectors was determined by a detailed GEANT4 simulation of the experimental setup. The parameters of the response functions were determined by simulating monoenergetic neutrons over a range of energies. The shape of the response function was determined primarily from high statistic experiments performed at ISOLDE in CERN [8]. The efficiency from this simulation set was benchmarked against experimental determination from a quasi-monoenergetic neutron beam using a method similar to that presented in Ref. [21].

III. ANALYSIS

Neutron energy was extracted by the neutron Time-of-Flight, nTOF, technique where the time it takes a neutron to travel a known distance is used to determine the neutron velocity, and subsequently energy. The TOF is derived from possible β particles from the amplified dynode signal on the YAP crystal timing as the start, and VANDLE signals as stops. The slowest neutrons observed in this experiment is around 160 ns in TOF, equivalent to 225 keV in neutron energy.

The standard data analysis method involves the generation of two-dimensional histograms where total light collected in the scintillator (QDC) resulting from the interaction of neutrons or γ rays is plotted against their time of flight (TOF). Prompt γ rays following β decay are used to determine the reference point for neutron TOF analysis [9,21]. Geometrical corrections are implemented using methods described in Ref. [8]. For a given neutron energy the maximum light yield can be modeled using the Birk's formula [22]. This gives rise to a characteristic shape of the distribution of measured neutrons.

A. ^{72}Co decay analysis

This experiment cannot definitely interpret the ^{72}Co delayed neutron emission due to the existence of $(0^+, 1^+)$ and $(6^-, 7^-)$ β-decaying states, as well as the presence of the 499 keV isomer in ^{71}Ni shown in Fig. 2. Nevertheless, the delayed neutrons can still be measured. A shorter half-life leads to a better signal to background ratio as a shorter ion-β correlation-time is used.

The ^{72}Co decay illustrates how VANDLE identifies neutrons. Shown in Fig. 3 is the plot of the scintillator light

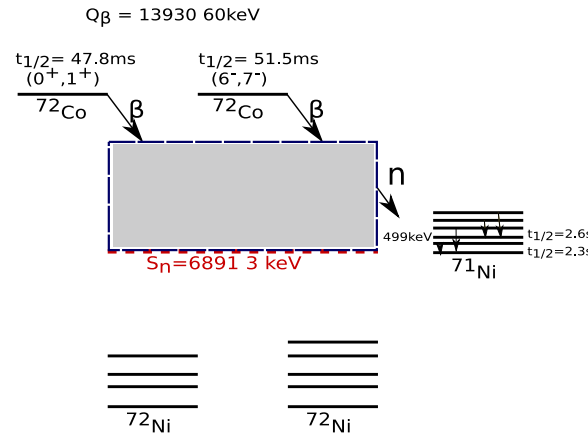

FIG. 2. Decay scheme for β decay of ^{72}Co isomeric states in ^{71}Ni are populated in β-delayed neutron emission.

yield (QDC) against the TOF. The black curve demonstrates the upper limit of light produced by neutrons. The peak at ≈ 4 ns is due to prompt γ rays passing the distance from the YAP detector to the VANDLE array from ^{72}Co β decay. The TOF of the prompt γ-ray peak, called the γ flash, is used to calibrate the neutron TOF for each detector.

In this experiment a projection of the plot from Fig. 3 is used to deconvolute the neutron spectrum. A limit on the TOF and the QDC is used to eliminate backgrounds and nonphysical results. The result of the neutron deconvolution from delayed neutron-emission of ^{72}Co is shown in Fig. 4. When there are relatively high-energy neutrons, background from the γ flash may spread into the high-energy neutron peaks.

The deconvolution of TOF ranges is primarily dependent on the peak width change with the neutron energy [8]. In this data set, relatively low statistics and background subtraction causes fluctuating TOF spectrum. The number of peaks and

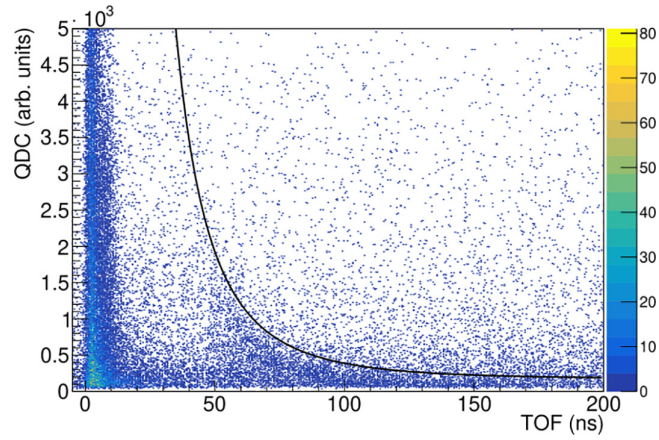

FIG. 3. Distribution of events from a γ or neutron for ^{72}Co with a 300 ms correlation time. The black curve is a function based on Birk's formula [22] describing the light generated by neutrons with that TOF [23,24]. Background was subtracted using negative time implant-β with negative values removed for clarity.

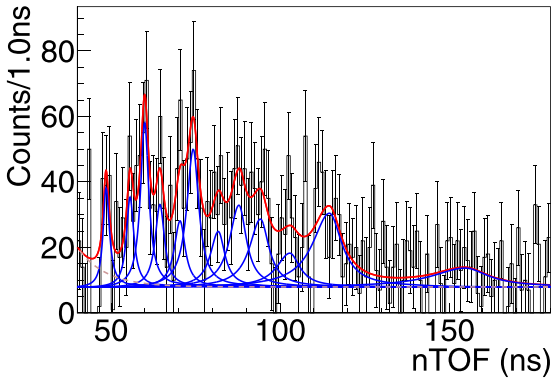

FIG. 4. Deconvolution of the observed ^{72}Co nTOF, with the total fit in red, and the individual peaks in blue, the dashed line is the background. Uncorrelated neutrons are removed using negative ion-β time correlation.

their location are selected such that the χ^2/NDF of the deconvolution is $\approx$ unity.

B. ^{70}Co decay analysis

The β-decaying $(6^-, 7^-)$ state of ^{70}Co has an evaluated half-life of 112 ± 7 ms, and several γ rays associated with this half-life, the most intense being the 969.7 keV γ ray [25] which is $4^+ \rightarrow 2^+$ and has a small contribution from the $(1^+, 2^+)$ [11] state. The 448.5 keV γ ray has a lower decay intensity than the 969.7 keV γ ray. The amount of efficiency of the HPGE detector results in grated counts for the 448.5 keV γ ray. The half-life for the $(6^-, 7^-)$ state was fit from the 448.5 keV γ ray. The 0–1 s negative-time subtracted γ-ray spectrum is in Fig. 5(a). The 448.5 keV γ-gated ion-β correlation time curve in Fig. 5(b) confirmed the $(6^-, 7^-)$ state β-decay half-life as 113 ± 7 (statistical) ms consistent with the evaluated half-life [25].

In order to eliminate accidental contributions from uncorrelated β signals in the ^{70}Co implant correlated spectrum, an implant-β correlation time from -1.0 s to 1.0 s was used. The events with negative correlation time contain only uncorrelated β signals. The low-spin isomer of ^{70}Co has a precise measured half-life [11] of 508 ± 7 ms.

The ion-β correlated curve with implanted ^{70}Co was first background subtracted using negative correlation time and then fit with an exponential function assuming contributions from both decays, with the high-spin $(6^-, 7^-)$ state decay half-life fixed to 113 ms from Fig. 5 and the low-spin $(1^+, 2^+)$ state decay half-life fixed to the published value of 508 ms [11] shown in Fig. 6. A fit was performed with an unfixed low-spin half-life, resulting in a value of 690 ± 150 ms consistent with the published value.

From fitting the ^{70}Co β decays using half-lives fixed to 113 ms and 508 ms the initial implantation population of the short-lived decay was found to be $53 \pm 6\%$ of the total number of implants from ^{70}Co. The approximately equal population is consistent with the ^{70}Co relative population from a previous experiment at the NSCL [13].

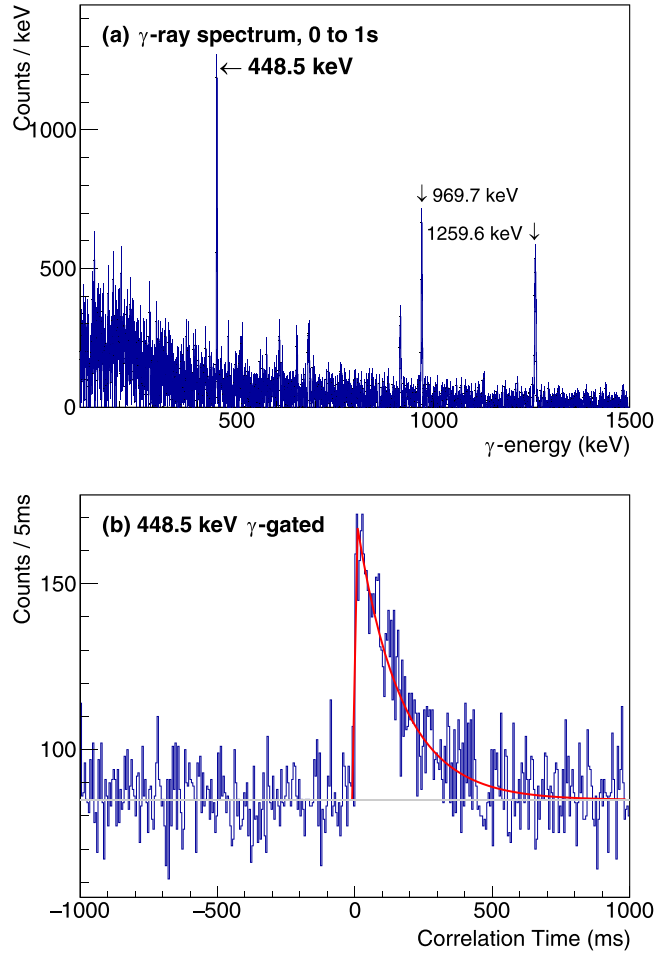

FIG. 5. (a) The 0–1 s γ-ray spectrum following ^{70}Co decay, background subtracted by negative ion-β correlation time. (b) Fit to the 448.5 keV γ-ray gated ion-β correlation time in ^{70}Ni, populated only by the β decay of the $(6^-, 7^-)$ state in ^{70}Co, results in a half-life of 113 ± 7 ms.

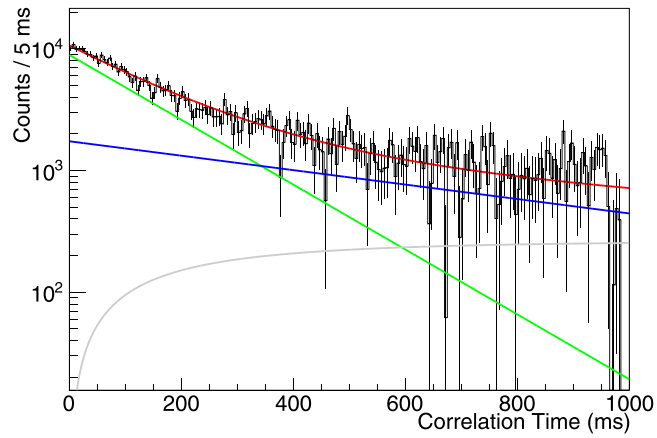

FIG. 6. Fit to the ion-β correlation time of ^{70}Co including the long-lived state decay (light blue) and the short-lived state decay (green), and a contribution from ^{70}Ni decay (black), populated by both decays of ^{70}Co.

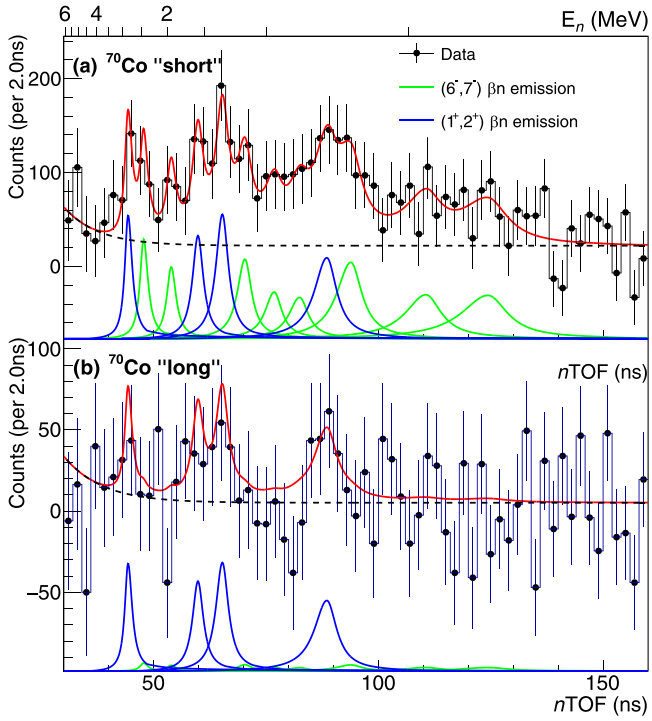

FIG. 7. (a)The ^{70}Co "short" nTOF spectrum. (b)The ^{70}Co "long" nTOF spectrum, consisting of the $(6^-, 7^-)$ state neutron emission in green, $(1^+, 2^+)$ state neutron emission in blue, with the total fit in red.

In order to analyze the neutron spectra with two states of different half-lives the positive implant-β correlation was divided into a 0.0 s to 0.5 s "short" segment, and a 0.5 s to 1.0 s "long" segment. The TOF data, shown in Fig. 7, in the "long" are almost entirely due to long-lived $(1^+, 2^+)$ state decay's neutron spectrum. This segment contains approximately 1/3 of long-lived decay counts and <5% of the short-lived decay counts. The "short" segment contains >95% of the short-lived $(6^-, 7^-)$ state decay counts, as well as approximately 2/3 the number of counts for the long-lived decay. The two histograms were fit simultaneously, taking into account the time evolution of the peak intensities associated with different half lives. The high-spin deconvolution includes structures clearly distinct from the low-spin deconvolution. Only the short-lived decay has neutrons with TOF longer than 107 ns equivalent to counts below 500 keV neutron energy, and counts fill in the long-lived neutron spectrum gap at 76 ns equivalent to 1 MeV neutrons.

Attribution of neutrons from the short-lived $(6^-, 7^-)$ state decay necessitated generation of the neutron-gated decay curve in ^{70}Co shown in Fig. 8. From this analysis it is clear that neutrons associated with the short-lived (high-spin) state decay are present. Uncertainty in the population from the decay curve requires the fit to the response function in order to attribute more clearly the number of neutrons from the long-lived (low-spin) and short-lived (high-spin) state decays.

IV. RESULTS

The peaks from Fig. 7 were used as input to a Hauser-Feshbach statistical model. The states populated by the neutron emission in order to produce the observed nTOF spectra were calculated with the BeOH Los Alamos code [26–29].

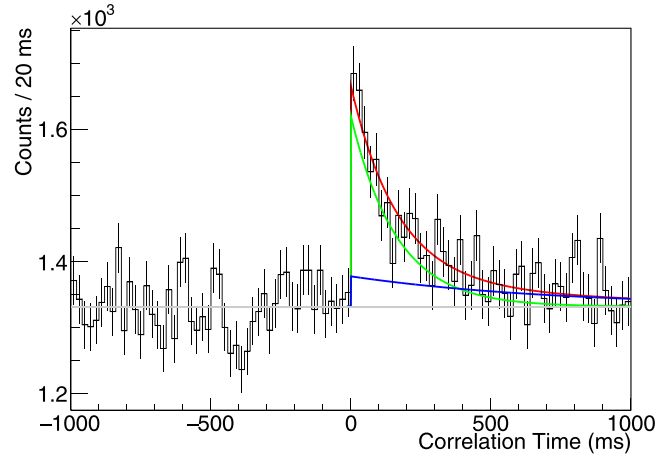

FIG. 8. Neutron-gated ion-β correlation time with the same nTOF range and cuts as the spectra in Fig. 7 with a fit to the long-lived decay (blue), and the short-lived decay (green), and a flat background associated with uncorrelated neutrons (gray) only for clarity.

The states populated by the neutron emission are determined by the angular momentum of the neutron and the phase-space from the available energy with $L = 1$ favored over higher L, and higher available energy favored. The term of "pseudolevel" from total absorption γ spectroscopy (TAS) [30,31] is used. In TAS pseudolevels describe an aggregate of states with varied decay paths. The pseudolevels used here are similar in that they use calculated possible paths following neutron emission. The states populated by the pseudolevels are calculated based on the energy and spin-parity of the states in ^{69}Ni. For all but the two highest excitation high-spin $(5^-, 6^-, 7^-)$ pseudolevels shown in Fig. 9, with the eight plots on the left side showing neutron-emitting pseudolevels from the $(6^-, 7^-)$ state in ^{70}Co following β decay, and the four plots on the right side showing the pseudolevels from the $(1^+, 2^+)$ state β decay. The neutron emission from the $(6^-, 7^-)$ decay is expected to only populate the $(9/2^+)$ ground state of ^{69}Ni. The $E^* = 9267$ keV ^{70}Ni excited pseudolevel has a small contribution from the $(5/2^-)$ 915 keV state. While the $E^* = 9796$ keV ^{70}Ni excited pseudolevel has a contribution from the $(9/2^-)$ 1959 keV state.

The low-spin $(0^+, 1^+, 2^+)$ pseudolevels have fine structure. All levels primarily populate the $(1/2^-)$ 321 keV isomer in ^{69}Ni, as well as small contributions from the $(9/2^+)$ ground state, and when energetically possible the $(5/2^-)$ 915 keV state.

The "fine structure" of the neutron emissions is taken into account in the nTOF spectrum deconvolutions at the top of Fig. 9.

From the efficiency corrected neutron deconvolution of the nTOF spectra compared with the β counts, I_β for the states were directly measured. The neutron-emission probability, P_n, as well as the states populated by the neutron emission were different for the $(1^+, 2^+)$ and $(6^-, 7^-)$ state β decays. From

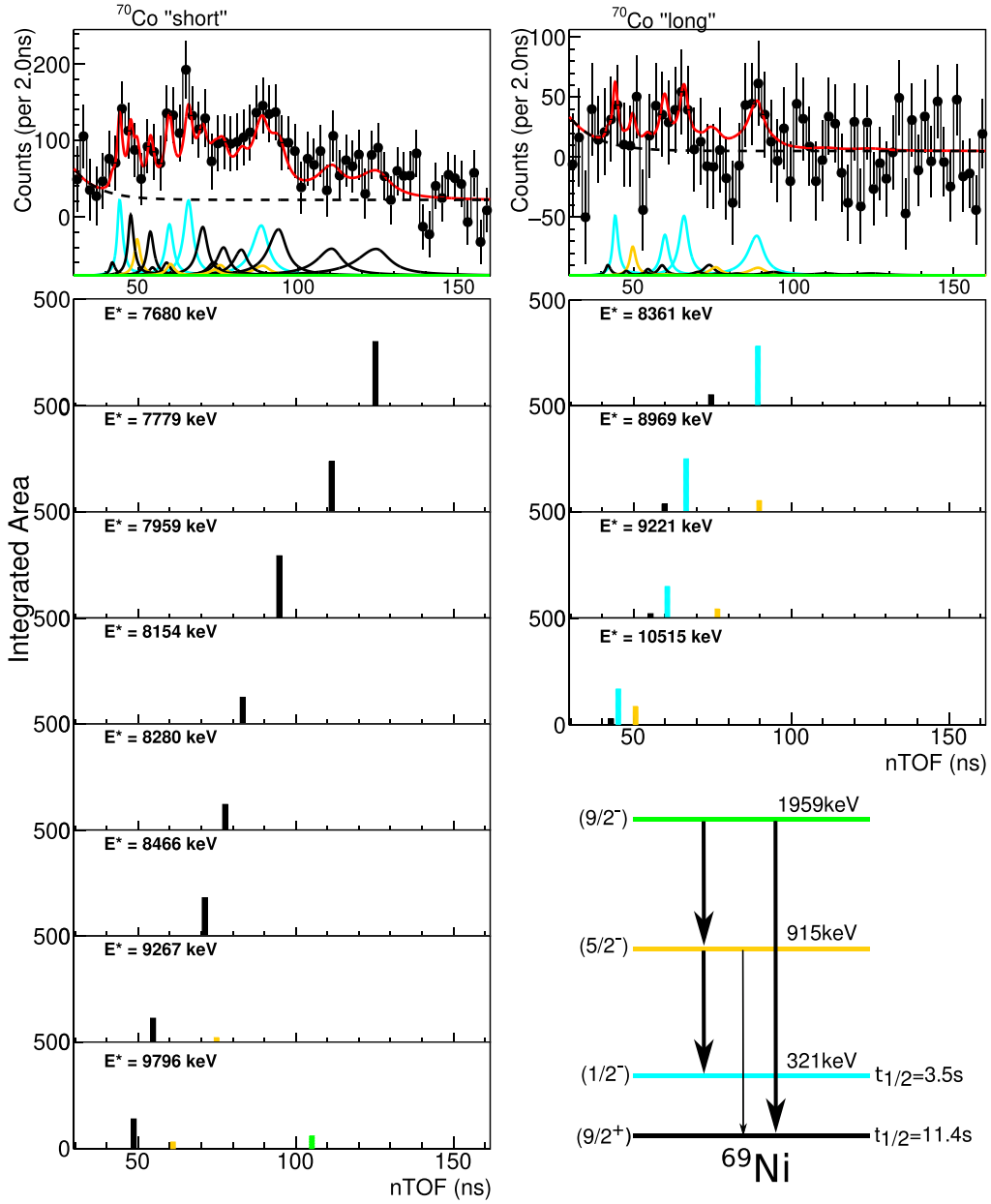

FIG. 9. Hauser-Feshbach prediction of the pseudolevels in ^{70}Ni populated in the decays of the short-lived 7^- (left) and long-lived 1^+ states in ^{70}Co. The contributions are color coded by the levels in the inset ^{69}Ni levels on the bottom right.

the I_β and the excitation energy in ^{70}Ni, the Gamow-Teller strength of the β transition, B(GT) is calculated. The I_β and B(GT) are shown in Fig. 10 and tabulated in Table I.

The levels in Table I are listed as single peaks, but most if not all, are multiple peaks across the uncertainty. In this case, the sum I_β and B(GT) across each peak range would remain unchanged within the associated uncertainty.

V. INTERPRETATION

This experiment was compared with shell-model calculations, the cumulative B(GT) below the neutron separation energy was compared with the ca48mh residual interactions that was fit to bound state γ-ray information from other publications [11,32] with a quenching of 20%. The data from the ^{70}Ni neutron-unbound pseudolevels, as well as the calculation and other experimental results are shown in Fig. 11.

The cumulative B(GT) of the neutron-emission data must be offset in order to compare with theory as the neutron-emission only describes B(GT) above the neutron-separation energy. The offset used was the value of the associated ca48mh theory at 7532 keV equivalent to 160 ns neutrons, the minimum used in the deconvolution,

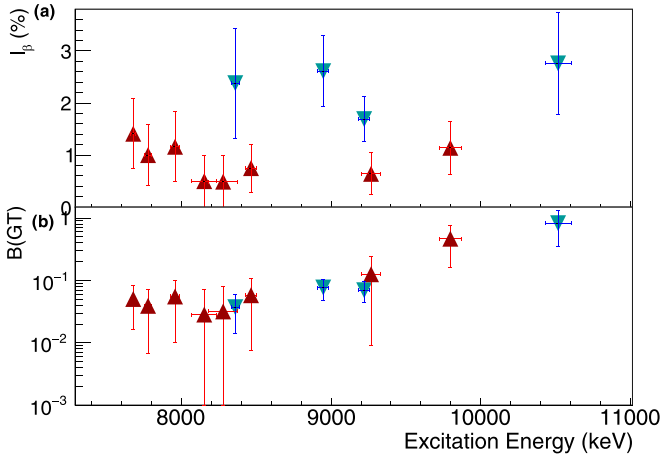

FIG. 10. (a) I_β and (b) B(GT) for the identified pseudolevel excited states in ^{70}Ni from nTOF, states for the low-spin isomer are shown in blue, and the high-spin are shown in red.

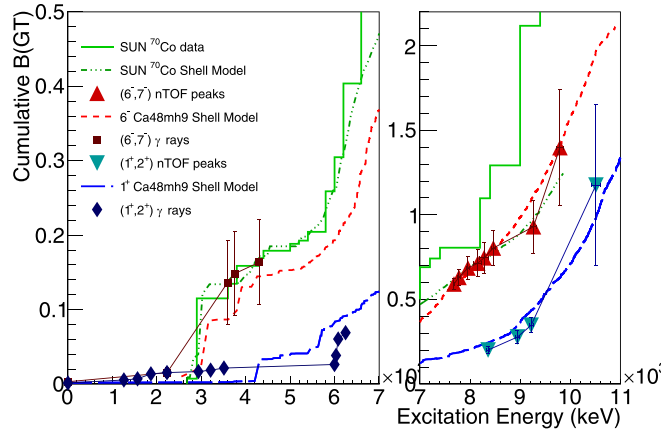

FIG. 11. The cumulative B(GT) for ^{70}Co β-decay transitions, the SUN data and shell model are from [18], the γ-ray data [7,32], and the ^{70}Ni excited pseudolevels from nTOF. Shown on the left are the shell-model calculations compared with the discrete γ-ray data, and on the right shell-model calculations compared with the ^{70}Ni excited pseudolevels from nTOF.

above the neutron-separation energy of ^{70}Ni. The availability of equivalent TAS measurements for both the $(6^-, 7^-)$ and $(1^+, 2^+)$ decays of ^{70}Co would allow offset of the neutron-emission cumulative B(GT) by data rather than solely by calculations. It is also possible that neutrons with energies below the detectable energy in this experiment were missed.

The ca48mh residual interaction used employs proton $1f_{7/2}$ (-18.56), $1f_{5/2}$ (-14.94), $2p_{3/2}$ (-13.44), $2p_{1/2}$ (-12.04), and neutron $1f_{5/2}$ (-8.39), $2p_{1/2}$ (-7.21), $1g_{9/2}$ (-5.26) single particle levels, with energies in MeV in parentheses. Single particle energies were adjusted to fit experimental data and the low-energy strength distribution. This model space does not have the complexity to generate deformation, but it produces B(GT) surprisingly consistent with the experimental data. The effective $Z = 28$ proton shell gap in ^{70}Ni amounts to only 2.9 MeV.

TABLE I. ^{70}Ni excited pseudolevels fit from the ^{70}Co nTOF spectra.

^{70}Co J_i	^{70}Ni E_{ex}(keV)	I_β(%)	B(GT)
$(6, 7^-)$	9796(73)	1.1(5)	0.47(31)
	9267(62)	0.6(4)	0.13(12)
	8466(36)	0.8(5)	0.06(05)
	8280(96)	0.5(5)	0.03(05)
	8154(83)	0.5(5)	0.03(04)
	7959(32)	1.2(7)	0.06(05)
	7779(22)	1.0(6)	0.04(03)
	7680(16)	1.4(7)	0.05(03)
	P_n	7.1(15)	
$(1, 2^+)$	10515(87)	2.8(10)	0.83(05)
	9221(38)	1.7(4)	0.07(03)
	8969(36)	2.6(7)	0.08(03)
	8361(26)	2.4(11)	0.04(02)
	P_n	9.4(17)	

Within the spherical shell model, the dominant configuration of the ^{70}Co ground state consists of a proton hole in the $\pi f_{7/2}$ orbital, and three neutrons in $\nu g_{9/2}$. The allowed Gamow-Teller transitions in the decay of ^{70}Co has two main components, which are separated in energy and can be linked to transformation between proton and neutron spin-orbit partners including fpg orbitals. The shell-model picture of the decay of $(6^-, 7^-)$ ^{70}Co is shown in Fig. 12. The dominant component can be explained as the transformation of a $f_{5/2}$ neutron into a $f_{7/2}$ proton, which is enabled by the proton vacancy in $Z = 27$ cobalt. This component is observed in the decays of Co isotopes, and the strength distribution is spread among relatively few states. TAS data [18] show clearly this transition has a peak around 3.5 MeV. The excited states in nickel isotopes populated in this transformation are typically neutron bound. The second component has a weaker contribution to the overall decay probability because it includes transition to states with significantly higher excitation energy and is therefore suppressed by the effects of the phase space.

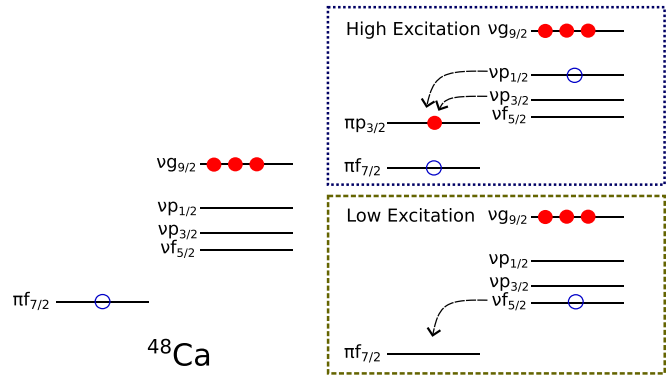

FIG. 12. Shell-model levels involved in the high-spin Gamow-Teller decay of ^{70}Co, with low excitation shown bottom right, and high excitation shown in top right.

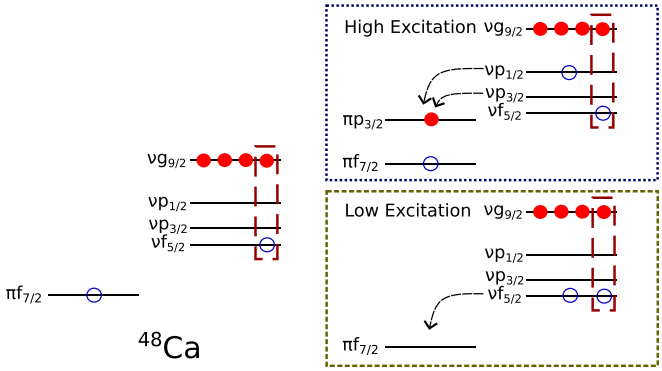

FIG. 13. Shell-model levels involved in the low-spin Gamow-Teller decay of ^{70}Co in the spherical picture, with low excitation shown bottom right, and high excitation shown in top right.

This includes the transformation of $f_{5/2}$, $p_{1/2}$, $p_{3/2}$, and $g_{9/2}$ neutrons into protons within the same orbitals. In the $Z = 27$ cobalt decays, these transitions are populating proton orbitals outside the $Z = 28$ closed shell and the extra excitation energy is approximately given by the size above the proton $f_{7/2}$ orbital. Due to a large number of possible combinations of shell-model configurations, the expected strength distribution has a semicontinuum character. It leads to a population of states at higher excitation energy in nickel isotopes which are typically neutron unbound.

The spherical shell-model forms a $(1^+, 2^+)$ state in ^{70}Co by promoting one of the fp neutrons into the $g_{9/2}$ orbital resulting in a positive parity state coupled $(\nu g_{9/2})^4$ shown in Fig. 13. With the $p_{1/2}$ orbital being nearest the Fermi surface, one might expect a low-lying 3^+ state with a $\pi f_{7/2}^{-1}$, $\nu p_{1/2}^{-1}$ dominant configuration. The decay of such a state would generally follow a similar pattern as for the high-spin state decay, with the dominant $\nu f_{5/2} \rightarrow \pi f_{7/2}$ transformation at lower energy and high $fpg \rightarrow fpg$ continuum at higher energy. The ^{70}Fe decay study [11] indicates that the long-lived positive parity isomeric state has a spin of 1^+ or 2^+.

The experimental data from neutron spectroscopy can be made to agree with the theory for the high energy part. The low-energy part of the low-spin decay, which was extracted from high-resolution γ-ray spectroscopy, has different behavior. The expected $\nu f_{5/2} \rightarrow \pi f_{7/2}$ do not appear at lower energies than 6 MeV [32]. The nonobservation of this transition could be attributed to the effect of deformation.

The calculation using ca48mh interactions also reasonably describes the experimental data for the low-spin isomer decay. The strength distribution for the low-spin decay is shifted to higher energies because the dominant configurations for low-spin positive parity states populated in GT decay include $(g_9/2)^4_J = 0$ configuration. In addition, the $\nu f_{5/2} \rightarrow \pi f_{7/2}$ transition, which is dominant in the high-spin decay, is suppressed and shifted to higher energies. Both effects conspire to generate a longer lifetime for the decay of the positive parity state. The experimental data from high-resolution γ-ray spectroscopy indicate that this transition is at 6 MeV and appears close to the spherical shell-model prediction. The Monte Carlo shell model was employed to calculate the ^{70}Ni structure with a large amount of included configurations and generated low-energy deformed structures [11]. In that case, the lowest excited low-spin states are deformed; presently, results of this method for strength distribution are unavailable.

VI. CONCLUSIONS

In this experiment, the first ever neutron spectroscopy of the ^{70}Co $(6^-, 7^-)$ and $(1^+, 2^+)$ β-decaying states was performed. These data indicate several exciting aspects of the decay of ^{70}Co. The observed neutron emission indicates significant differences in the neutron-energy spectra of the high- and low-spin decays, though they are statistics limited.

In both cases, neutron emission reveals the part of the decay strength dominated by the transformation of the neutrons occupying the fp orbitals to fp protons above the $Z = 28$ shell closure. Shell-model calculations generate strength distribution, which is consistent with the experiment. The shell-model interpretation explains the half-life difference between high and low-spin isomers caused by shifting the strength distribution to higher energies for low-spin states.

The data does not exclude the deformation effects needed to generate a low-spin isomeric state in ^{70}Co. The population of excited states across the $Z = 28$ proton shell gap causes the rapid increase in the strength distribution observed in both decays. The effective shell gap in ^{70}Ni is determined to be 2.9 MeV.

For the $(6^-, 7^-)$ ^{70}Co β decay, direct observation of neutrons, while not entirely inconsistent with the SuN TAS result [18], does change the degree and interpretation of neutron-γ competition in this decay. Definite statements are beyond the statistical accuracy of this experiment.

The indications of discrepancies can only be resolved by a new measurement; a high-statistics experiment combining total absorption and neutron spectroscopy is planned at the Facility for Rare Isotope Beams (FRIB) utilizing the FRIB Decay Station Initiator.

ACKNOWLEDGMENTS

This research was sponsored in part by the Office of Nuclear Physics, U.S. Department of Energy under Awards No. DE-FG02-96ER40983 (UTK) and No. DE-AC05-00OR22725 (ORNL), and by the National Nuclear Security Administration under the Stewardship Science Academic Alliances program through DOE Awards No. DE-NA0003899 and No. DE-NA0004068, U.S. Department of Energy, National Nuclear Security Administration, Grant No. DE-NA0004068, and National Science Foundation under Grant No. PHY 1848177 (CAREER).

[1] T. Otsuka, T. Suzuki, R. Fujimoto, H. Grawe, and Y. Akaishi, Evolution of nuclear shells due to the tensor force, Phys. Rev. Lett. **95**, 232502 (2005).

[2] R. Broda, B. Fornal, W. Królas, T. Pawłat, D. Bazzacco, S. Lunardi, C. Rossi-Alvarez, R. Menegazzo, G. de Angelis, P. Bednarczyk, J. Rico, D. De Acuña, P. J. Daly, R. H. Mayer,

M. Sferrazza, H. Grawe, K. H. Maier, and R. Schubart, $N = 40$ neutron subshell closure in the ^{68}Ni nucleus, Phys. Rev. Lett. **74**, 868 (1995).

[3] A. Gade, R. V. F. Janssens, T. Baugher, D. Bazin, B. A. Brown, M. P. Carpenter, C. J. Chiara, A. N. Deacon, S. J. Freeman, G. F. Grinyer, C. R. Hoffman, B. P. Kay, F. G. Kondev, T. Lauritsen, S. McDaniel, K. Meierbachtol, A. Ratkiewicz, S. R. Stroberg, K. A. Walsh, D. Weisshaar *et al.*, Collectivity at $N = 40$ in neutron-rich ^{64}Cr, Phys. Rev. C **81**, 051304(R) (2010).

[4] F. Recchia, S. M. Lenzi, S. Lunardi, E. Farnea, A. Gadea, N. Mărginean, D. R. Napoli, F. Nowacki, A. Poves, J. J. Valiente-Dobón, M. Axiotis, S. Aydin, D. Bazzacco, G. Benzoni, P. G. Bizzeti, A. M. Bizzeti-Sona, A. Bracco, D. Bucurescu, E. Caurier, L. Corradi *et al.*, Spectroscopy of odd-mass cobalt isotopes toward the $N = 40$ subshell closure and shell-model description of spherical and deformed states, Phys. Rev. C **85**, 064305 (2012).

[5] S. Suchyta, S. N. Liddick, Y. Tsunoda, T. Otsuka, M. B. Bennett, A. Chemey, M. Honma, N. Larson, C. J. Prokop, S. J. Quinn, N. Shimizu, A. Simon, A. Spyrou, V. Tripathi, Y. Utsuno, and J. M. VonMoss, Shape coexistence in ^{68}Ni, Phys. Rev. C **89**, 021301(R) (2014).

[6] T. Lokotko, S. Leblond, J. Lee, P. Doornenbal, A. Obertelli, A. Poves, F. Nowacki, K. Ogata, K. Yoshida, G. Authelet, H. Baba, D. Calvet, F. Château, S. Chen, A. Corsi, A. Delbart, J.-M. Gheller, A. Gillibert, T. Isobe, V. Lapoux *et al.*, Shell structure of the neutron-rich isotopes ^{69,71,73}Co, Phys. Rev. C **101**, 034314 (2020).

[7] A. Morales, G. Benzoni, H. Watanabe, Y. Tsunoda, T. Otsuka, S. Nishimura, F. Browne, R. Daido, P. Doornenbal, Y. Fang, G. Lorusso, Z. Patel, S. Rice, L. Sinclair, P.-A. Söderström, T. Sumikama, J. Wu, Z. Xu, A. Yagi, R. Yokoyama *et al.*, Type II shell evolution in A = 70 isobars from the N $\geqslant$ 40 island of inversion, Phys. Lett. B **765**, 328 (2017).

[8] Z. Y. Xu, M. Madurga, R. Grzywacz, T. T. King, A. Algora, A. N. Andreyev, J. Benito, T. Berry, M. J. G. Borge, C. Costache, H. De Witte, A. Fijalkowska, L. M. Fraile, H. O. U. Fynbo, A. Gottardo, C. Halverson, L. J. Harkness-Brennan, J. Heideman, M. Huyse, A. Illana *et al.*, β-delayed neutron spectroscopy of ^{133}In, Phys. Rev. C **108**, 014314 (2023).

[9] Z. Y. Xu, M. Madurga, R. Grzywacz, T. T. King, A. Algora, A. N. Andreyev, J. Benito, T. Berry, M. J. G. Borge, C. Costache, H. De Witte, A. Fijalkowska, L. M. Fraile, H. O. U. Fynbo, A. Gottardo, C. Halverson, L. J. Harkness-Brennan, J. Heideman, M. Huyse, A. Illana *et al.*, ^{133}In: A Rosetta stone for decays of *r*-process nuclei, Phys. Rev. Lett. **131**, 022501 (2023).

[10] W. F. Mueller, B. Bruyneel, S. Franchoo, M. Huyse, J. Kurpeta, K. Kruglov, Y. Kudryavtsev, N. V. S. V. Prasad, R. Raabe, I. Reusen, P. Van Duppen, J. Van Roosbroeck, L. Vermeeren, L. Weissman, Z. Janas, M. Karny, T. Kszczot, A. Płochocki, K.-L. Kratz, B. Pfeiffer *et al.*, Shell structure of the neutron-rich isotopes ^{69,71,73}Co, Phys. Rev. C **61**, 054308 (2000).

[11] A. I. Morales, A. Algora, B. Rubio, K. Kaneko, S. Nishimura, P. Aguilera, S. E. A. Orrigo, F. Molina, G. de Angelis, F. Recchia, G. Kiss, V. H. Phong, J. Wu, D. Nishimura, H. Oikawa, T. Goigoux, J. Giovinazzo, P. Ascher, J. Agramunt, D. S. Ahn *et al.*, Simultaneous investigation of the $T = 1(J^\pi = 0^+)$ and $T = 0(J^\pi = 9^+)\beta$ decays in ^{70}Br, Phys. Rev. C **95**, 064327 (2017).

[12] M. Sawicka, R. Grzywacz, I. Matea, H. Grawe, M. Pfützner, J. M. Daugas, M. Lewitowicz, D. L. Balabanski, F. Becker, G. Bélier, C. Bingham, C. Borcea, E. Bouchez, A. Buta, M. La Commara, E. Dragulescu, G. de France, G. Georgiev, J. Giovinazzo, M. Górska *et al.*, Low energy levels in ^{72}Ni, Phys. Rev. C **68**, 044304 (2003).

[13] C. J. Prokop, B. P. Crider, S. N. Liddick, A. D. Ayangeakaa, M. P. Carpenter, J. J. Carroll, J. Chen, C. J. Chiara, H. M. David, A. C. Dombos, S. Go, J. Harker, R. V. F. Janssens, N. Larson, T. Lauritsen, R. Lewis, S. J. Quinn, F. Recchia, D. Seweryniak, A. Spyrou *et al.*, New low-energy 0^+ state and shape coexistence in ^{70}Ni, Phys. Rev. C **92**, 061302(R) (2015).

[14] W. F. Mueller, B. Bruyneel, S. Franchoo, H. Grawe, M. Huyse, U. Köster, K.-L. Kratz, K. Kruglov, Y. Kudryavtsev, B. Pfeiffer, R. Raabe, I. Reusen, P. Thirolf, P. Van Duppen, J. Van Roosbroeck, L. Vermeeren, W. B. Walters, and L. Weissman, Magicity of the ^{68}Ni semidouble-closed-shell nucleus probed by Gamow-Teller decay of the odd-*A* neighbors, Phys. Rev. Lett. **83**, 3613 (1999).

[15] R. Surman, M. Mumpower, and A. Aprahamian, The Sensitivity of *r*-Process Nucleosynthesis to Individual β-delayed Neutron Emission Probabilities, *Proceedings of the Conference on Advances in Radioactive Isotope Science (ARIS2014)* (The Physical Society of Japan, 2015), p. 010010.

[16] G. W. Misch, S. K. Ghorui, P. Banerjee, Y. Sun, and M. R. Mumpower, Astromers: Nuclear isomers in astrophysics, Astrophys. J. Suppl. Series **252**, 2 (2021).

[17] A. Algora, B. Rubio, D. Cano-Ott, J. L. Taín, A. Gadea, J. Agramunt, M. Gierlik, M. Karny, Z. Janas, A. Płochocki, K. Rykaczewski, J. Szerypo, R. Collatz, J. Gerl, M. Górska, H. Grawe, M. Hellström, Z. Hu, R. Kirchner, M. Rejmund *et al.*, (GSI Euroball Collaboration), Fine structure of the Gamow-Teller resonance revealed in the decay of ^{150}Ho 2^- isomer, Phys. Rev. C **68**, 034301 (2003).

[18] A. Spyrou, S. N. Liddick, F. Naqvi, B. P. Crider, A. C. Dombos, D. L. Bleuel, B. A. Brown, A. Couture, L. Crespo Campo, M. Guttormsen, A. C. Larsen, R. Lewis, P. Möller, S. Mosby, M. R. Mumpower, G. Perdikakis, C. J. Prokop, T. Renstrøm, S. Siem, S. J. Quinn *et al.*, Strong neutron-γ competition above the neutron threshold in the decay of ^{70}Co, Phys. Rev. Lett. **117**, 142701 (2016).

[19] D. Morrissey, B. Sherrill, M. Steiner, A. Stolz, and I. Wiedenhoever, Commissioning the A1900 projectile fragment separator, Nucl. Instrum. Methods Phys. Res. B **204**, 90 (2003).

[20] H. O. Anger, Scintillation camera, Rev. Sci. Instrum. **29**, 27 (1958).

[21] W. Peters, S. Ilyushkin, M. Madurga, C. Matei, S. Paulauskas, R. Grzywacz, D. Bardayan, C. Brune, J. Allen, J. Allen, Z. Bergstrom, J. Blackmon, N. Brewer, J. Cizewski, P. Copp, M. Howard, R. Ikeyama, R. Kozub, B. Manning, T. Massey *et al.*, Performance of the versatile array of neutron detectors at low energy (VANDLE), Nucl. Instrum. Methods Phys. Res. A **836**, 122 (2016).

[22] J. Birks, Scintillations from organic crystals: Specific fluorescence and relative response to different radiations, Proc. Phys. Soc. A **64**, 874 (1951).

[23] J. Heideman, Study of 134In beta-delayed neutron emission and development of a new generation neutron detector, Ph.D. thesis, University of Tennessee, Knoxville, 2021.

[24] R. Madey, F. M. Waterman, A. R. Baldwin, J. N. Knudson, J. Carlson, and J. Rapaport, The response of NE-228A, NE-228,

NE-224, and NE-102 scintillators to protons from 2.43 to 19.55 MeV, Nucl. Instrum. Methods **151**, 445 (1978).

[25] G. Gürdal and E. McCutchan, Nuclear data sheets for A = 70, Nucl. Data Sheets **136**, 1 (2016).

[26] T. Kawano, P. Talou, M. B. Chadwick, and T. Watanabe, Monte Carlo simulation for particle and γ-ray emissions in statistical Hauser-Feshbach model, J. Nucl. Sci. Technol. **47**, 462 (2010).

[27] T. Kawano, R. Capote, S. Hilaire, and P. Chau Huu-Tai, Statistical Hauser-Feshbach theory with width-fluctuation correction including direct reaction channels for neutron-induced reactions at low energies, Phys. Rev. C **94**, 014612 (2016).

[28] T. Kawano, Unified coupled-channels and Hauser-Feshbach model calculation for nuclear data evaluation, arXiv:1901.05641.

[29] A. E. Lovell, T. Kawano, S. Okumura, I. Stetcu, M. R. Mumpower, and P. Talou, Extension of the Hauser-Feshbach fission fragment decay model to multichance fission, Phys. Rev. C **103**, 014615 (2021).

[30] J. L. Tain and D. Cano-Ott, The influence of the unknown de-excitation pattern in the analysis of β-decay total absorption spectra, Nucl. Instrum. Methods Phys. Res. A **571**, 719 (2007).

[31] R. Greenwood, R. Helmer, M. Lee, M. Putnam, M. Oates, D. Struttmann, and K. Watts, Total absorption gamma-ray spectrometer for measurement of beta-decay intensity distributions for fission product radionuclides, Nucl. Instrum. Methods Phys. Res. A **314**, 514 (1992).

[32] G. Benzoni, Investigation of ^{70,72,74}Ni from β decay of ^{70,72,74}Co, *Nuclear Structure Conference 2016* (2016).